Available online at www.sciencedirect.com

ScienceDirect

Ceramics International 40 (2014) 3305–3313

CERAMICS INTERNATIONAL

www.elsevier.com/locate/ceramint

Water purification and toxicity control of chlorophenols by 3D nanofiber membranes decorated with photocatalytic titania nanoparticles

Seongpil An[a,1], Min Wook Lee[a,1], Bhavana N. Joshi[a], Ayeong Jo[b], Jinho Jung[b], Sam S. Yoon[a,*]

[a]School of Mechanical Engineering, Korea University, Seoul 136-713, Republic of Korea
[b]Division of Environmental Science & Ecological Engineering, Korea University, Seoul 136-713, Republic of Korea

Received 9 September 2013; received in revised form 23 September 2013; accepted 23 September 2013
Available online 7 October 2013

Abstract

Highly photocatalytic water purification three-dimensional nanofiber membranes were fabricated. We identified the optimal fabrication process of nylon-6 nanofiber membranes suspending titania nanoparticles for potential water purifications and toxicity control of chlorophenols. Nanofibers and nanoparticles were deposited on a soda lime glass substrate by electrospinning and electrospraying, respectively. Titania nanoparticles were used to induce the UV light driven photocatalytic effect and nanofibers were used to tightly suspend the nanoparticles in air. Both batch and continuous deposition processes were introduced in the membrane fabrication process and their water purification performances were compared and quantified using a methylene blue solution, which is often used as a model pollutant. Surface morphologies and characteristics of the membranes fabricated at various process conditions were also provided. The membrane fabricated by the continuous means yielded 100% degradation of the methylene blue solution within 90 min under a relatively weak UV irradiation (0.6 mW/cm^2), which promises its potential indoor application. The nano-textured membranes developed in this work was also applied to the real pollutants, such as chlorophenols, and showed a promising performance in their toxicity control.

Keywords: Nanofibers; Titania; Photocatalysis; Water purification; Toxicity control

1. Introduction

Water purification technology currently relies heavily on the use of gravel, sand filters, and chlorine, which tend to be not only bulky but also expensive because of disposal requirements for waste filters and possible additional chemical treatment [1,2]. Alternatively, titania photocatalysis from exposure of titania to ultra-violet (UV) light can be regarded as an appropriate disinfection method because of titania's strong oxidizing capabilities [3–6]. In addition, titania is cheap and abundant, chemically stable, non-photo-degradable, nontoxic, manufacturable at atmospheric conditions [7,8] and photo-inducible by natural sunlight without exposure to manmade UV light [9] and thus it is economically viable and environmentally friendly [10].

Because photocatalysis is an interfacial phenomenon [11], purification performance can be maximized when the active surface-area-to-volume ratio is maximized. The maximization of the active surface-area-to-volume ratio in turn facilitates efficient UV irradiance and high quantum yield [12]. The most obvious way to maximize the surface contact area is to disperse titania nanoparticles in an aqueous medium inside a fluidized reactor [13], known as the mobilized mode. However, this mobilized mode ultimately requires separation of the fine nanoparticles from the purified water, but this separation is difficult because fine powders remain in a colloidal state and do not sufficiently settle, requiring additional equipment [14].

To avoid this technical difficulty, an immobilized mode, such as the condition created by use of solid membranes (or films), is often proposed as an alternative [7,8]. Membranes are favorable because of their simple and low-cost manufacturability. However, membranes in general are 2D and have reduced active surface areas and, thus, their photocatalytic efficiency is lower than those of mobilized modes. A polymer-based nanofiber

*Corresponding author.
E-mail address: skyoon@korea.ac.kr (S.S. Yoon).
[1]Equal contribution.

0272-8842/$ - see front matter © 2013 Elsevier Ltd and Techna Group S.r.l. All rights reserved.
http://dx.doi.org/10.1016/j.ceramint.2013.09.104

membrane comprised of nanoparticles would possess the advantages of a 2D membrane and 3D nanoparticles; such a membrane can be fabricated by installation of electrospraying and electrospinning.

Electrospun nanofibers can construct 3D-structured water purification membrane simply by trapping or suspending nanoparticles between nanofibers. By controlling the amounts of nanoparticles and nanofibers and their morphological structures, both the photocatalytic surface area and membrane porosity can be optimized. Specifications of the membrane, such as size, porosity and morphology, can be controlled by controlling process parameters like the applied voltage [15–17], nozzle-to-collector distance [17,18] and material properties such as polymer concentration [18–20] and solvent evaporation rate [21,22]. Electrospun fiber membranes are used in tissue engineering [23,24], dye-sensitized solar cells electrodes [25,26], microarray [27,28], membrane fabrication [29,30], textiles [31], fuel cells [32] and water purification filters [33,34]. To the best of our knowledge, only few studies have investigated the use of nanofibers suspending nanoparticles for photocatalytic decomposition applications [35]. Lombardi et al. [35] electrospun polyamide-6 precursor containing titania and observed the photodegradation of methylene blue. Our unique installation of electrosprayed titania particles and electrospun nanofibers distinguishes our work from the previous effort [35] that did not take full advantage of 3D suspension of titania nanoparticle (P25); Lombardi et al. [35] mixed P25 with the polymeric solution and produced electrospun nanofibers. We will show that our unique installation of electrospraying and electrospinning is capable of producing membranes with significantly superior performance in photocatalytic decomposition, as compared to the membrane produced by the previous study [35].

We did not mix P25 with the polymeric solution. Rather, we deposited nanoparticles and nanofibers separately, making the full 3D suspension of P25 between nanofibers. It should be noted that the titania nanoparticles were used to induce the UV-driven photocatalytic activity and nanofibers were used to tightly suspend the nanoparticles. Two options were presented for this type of membrane fabrication in which the nanoparticles and nanofibers were deposited separately: the batch and the continuous process, as illustrated in Fig. 1. In the batch process, nanoparticles were initially electrosprayed onto a substrate and then nylon-6 nanofibers were electrospun on top of P25 to completely shield the nanoparticles. In the continuous process, nylon-6 nanofibers and titania nanoparticles were deposited simultaneously by electrospinning and electrospraying, respectively, onto a substrate attached to a rotating cylinder, making a truly 3D-structured water purification nanofiber membrane.

We will identify the surface morphologies and characteristics (such as diameters of nanofibers and nanoparticles) of the membranes fabricated at various parameter values of this combined process. The water purification performance of the membranes will be tested using a methylene blue (MB) solution, which is often used as a model pollutant as it decomposes by direct oxidation and due to the OH radicals generated during the photocatalytic process [36]. The real pollutants, such as chlorophenols, were also used to show their toxicity reduction after applying the 3D photocatalytic nanofiber membrane.

2. Experimental

The parameters that are involved in the membrane fabrication process include nozzle-to-substrate distance (S_1 and S_2), cylinder rotating speed (V_{RPM}), deposition time (t_{dep}), nozzle diameters, flowrate (Q_1 and Q_2), applied voltage (V_1 and V_2); see Fig. 1. The optimal flowrate and voltage are fixed according to the Taylor cone formation for the given nozzle diameters. The cylinder rotating speed and the deposition time are set to $V_{RPM}=300$ RPM and $t_{dep}=5$ min, respectively. Both batch and continuous fabrication processes are applied separately for membrane fabrication. The fabricated membranes are tested with MB photodegradation and the performance of each membrane is compared against the others. The membrane with the best water purification performance will be identified. Installation of multiple nozzles of electrospraying and electrospinning would provide the large scale production environment. However, we herein focused on the lab scale production of the membrane with moderately small mass flowrate of TiO_2 and nylon-6. It should be noted that our membrane can lose TiO_2 particles if the membrane is severely sonicated with the sonication frequency of 300 Hz or greater. For the water purification tests considered in this report, the membrane performed well without losing its structural stability; we did not observe any discernible TiO_2 particle detachment.

2.1. Electrospraying

Titania nanoparticles (P25-Daegusa, Germany) are a mixture of 80% anatase and 20% rutile, which were dispersed in ethanol solution to facilitate electrospraying. The average size and specific surface area was 21 nm and 50 m^2/g, respectively. The amount of titania nanoparticles was purposely set low ($\sim$3 wt%) to prevent precipitation and aggregation of the particles as much as possible. No special dispersant or surfactant was used. The precursor solution was supplied by a syringe pump comprising a nozzle with 4 mm diameter and the flowrate of $Q_1=1$ ml/h. Titania nanoparticles were electrosprayed toward the substrate within $t_{dep}=5$ min. The high voltage of $V_1=7$ kV was applied to the nozzle to form a Taylor cone produced atomization.

2.2. Electrospinning

The polymeric precursor for nanofiber production was prepared by dissolving 15 wt% nylon-6 pellet in formic acid (*Sigma-Aldrich*) and stirred vigorously to get homogenous solution. The precursor was supplied to the nozzle of 0.25 mm diameter by a syringe pump. The flowrate was $Q_2=0.1$ ml/h with the standoff distance of $S_2=6$ and 7 cm. The applied voltage was $V_2=9$ kV which produced nylon-6 nanofibers deposited onto a soda lime glass substrate (3×3 cm^2). The nylon-6 fibers promote the strong adherence of titania nanoparticles to the substrate, which will be shown in later sections.

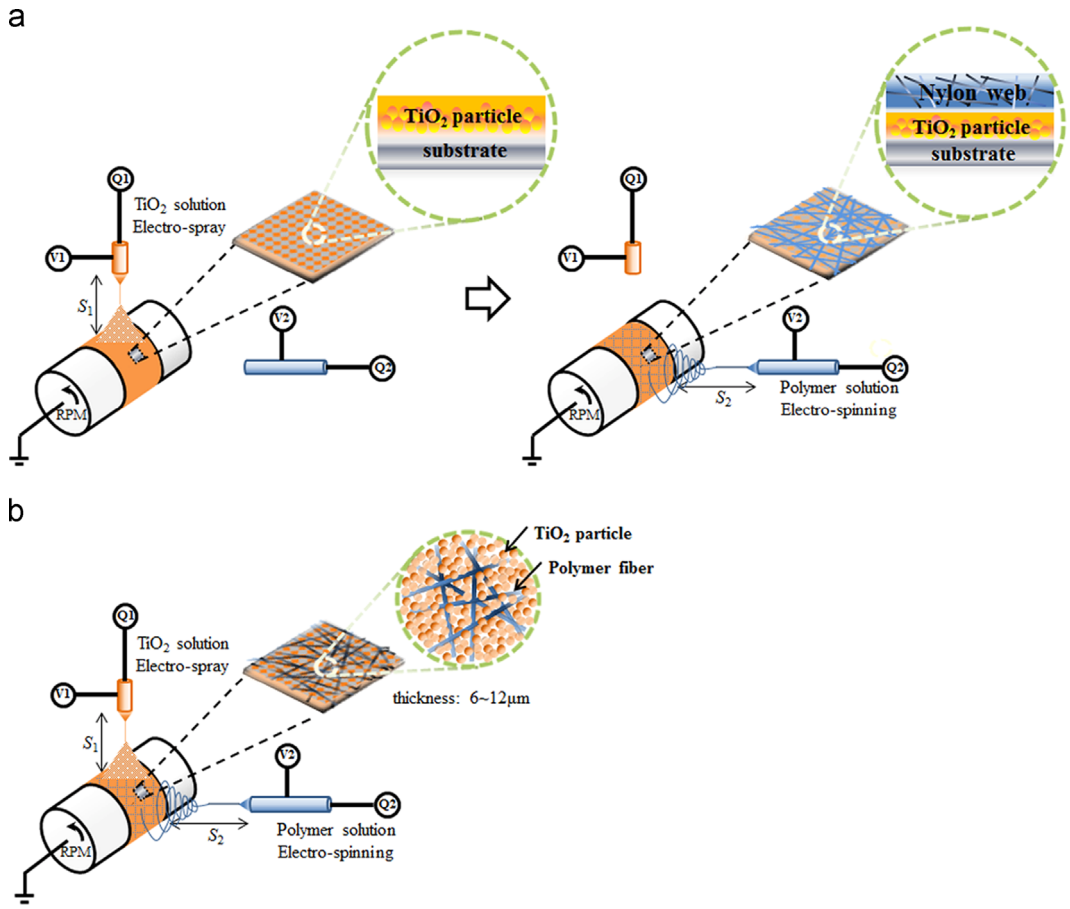

Fig. 1. Schematic (a) batch process (2D structure) and (b) continuous process (3D structure).

2.3. Batch and continuous processes

Fig. 1(a) and (b) shows the fabrication process of the nanofiber membranes by the batch and continuous processes, respectively. The same amounts of nanoparticles and nanofibers are deposited to give comparable water purification performances.

In the batch process, titania nanoparticles were first deposited onto a substrate and then nanofibers were electrospun to shield the nanoparticles on top, as illustrated in Fig. 1(a). In result, this batch process produces a membrane of 2D structure. Conversely, in the continuous process, as depicted in Fig. 1(b), the nylon-6 solution was electrospun horizontally while the ethanol solution containing dispersed titania nanoparticles was electrosprayed vertically toward the glass substrate attached to the cylinder rotating at 300 RPM. The nozzle-to-substrate standoff distances, S_1 and S_2, are important process parameters because they determine the morphology and structure of the membrane.

2.4. Membrane characterizations

The microstructures of the titania suspending nanofiber membranes were characterized by a high-resolution scanning electron microscope (SEM, Hitachi S-5000). The average diameters of the nanoparticles and nanofibers were identified using SEM images. UV light (0.6 mW/cm^2, 365 nm, VILBER LOURMAT, France) was used to induce the photocatalytic effect of titania nanoparticles. All membranes were kept inside a dark box for 24 h prior to any UV light illumination test to eliminate the remaining photocatalytic effect. The UV light illumination time was $t_{UV}=90$ min. All cases were repeated at least three times to ensure experimental repeatability. Note, that all of the electrospun in this study were fabricated by deposition for $t_{dep}=5$ min without any further post-treatment.

2.5. Methylene blue photodegradation test

Methylene blue (MB) solution is often used as a model pollutant as it decomposes by direct oxidation and due to the OH radicals generated during the photocatalytic process [37]. MB solution (#M2661, 0.1 wt% solution in water, *Samchun Chemical*, Korea) was mixed with deionized water at a 1:200 volume ratio (5 ppm). The amount of MB solution used for each photodecomposition test was 1.7 ml. Titania-suspended nanofiber membranes that had been UV-irradiated for 90 min (wavelength 365 nm, intensity 0.6 mW/cm^2) were placed and sealed inside a Pyrex Petri dish. The concentration of MB inside the vessel was diluted as photocatalysis proceeded; its concentration was monitored by a UV–vis spectrophotometer (OPTIZEN POP, *Mecasys Co.* Ltd., Korea, $=190\leq\lambda\leq1100$ nm). Absorbance data from

UV–vis spectroscopy was obtained by converting transmittance data using the Beer–Lambert law [38].

2.6. Toxicity test of chlorophenols

2,4-dichlorophenol (2,4-DCP, $\geq 99\%$) and 2,4,6-trichlorophenol (2,4,6-TCP, $\geq 98\%$) were purchased from Sigma-Aldrich Co. (USA) and used without further purification. Aqueous solutions (5×10^{-4} M) were prepared with deionized water (DW) with a resistivity of 18.2 MΩ cm^{-1} (Puris, Esse-UP Water System; Mirae St Co., Korea). UV irradiation ($\lambda = 365$ nm and $I = 0.6$ mW/cm^2) was lasted for 3 h. A TiO_2-decorated nanofiber membrane was placed inside an open Pyrex Petri dish containing the aqueous solution.

Acute toxicity tests were carried out according to the Organization for Economic Co-operation and Development (OECD) standard procedure [39] using *Daphia magna* neonates (≤ 24 h old). One control and five or more dilutions of each sample with four replicates were prepared for the toxicity test, and then five neonates and 10 mL of test solution were added to each well, respectively. The photoperiod during testing was 16 h light: 8 h dark and the temperature was 20 ± 2 °C. Immobility (defined as no response to gentle agitation for 15 s) was recorded after 48 h. The results were used to calculate the EC_{50} values by probit analysis or the trimmed Spearman-Karber method. EC_{50} values were transformed to toxic units ($TU = 100\%/EC_{50}$) for comparisons between samples.

3. Results and discussion

3.1. 2D membrane structure of batch process

Fig. 2 shows the surface morphology of the membrane fabricated by electrospraying and electrospinning then via the batch process shown in Fig. 1(a). A 2D titania layer was deposited onto a glass substrate by electrospraying, during which the ethanol solvent was quickly evaporated, leaving only the nanoparticles. The deposition time was short that not all areas of the substrate were covered by titania nanoparticles. Then the nanofibers are deposited over the titania layer to shield the nanoparticles between the substrate and nanofibers. As a result, this formed a bilayer of nanoparticles and nanofibers. Though the nanofibers were quite densely deposited, the membrane was gas- and liquid-permeable so the surrounding medium could cross the nanofiber layer and become in contact with the titania nanoparticles to be subjected to the interfacial photocatalytic effect. In Fig. 2, the left lower corner shows the bilayer while the right upper corner shows the nanoparticles only. The image of these nanoparticles without the nanofibers on top was photographed by covering the right upper corner during the electrospinning deposition.

3.2. 3D membrane structure of continuous process

Fig. 3 shows the surface morphology of the membranes fabricated by the continuous process shown in Fig. 1(b). In

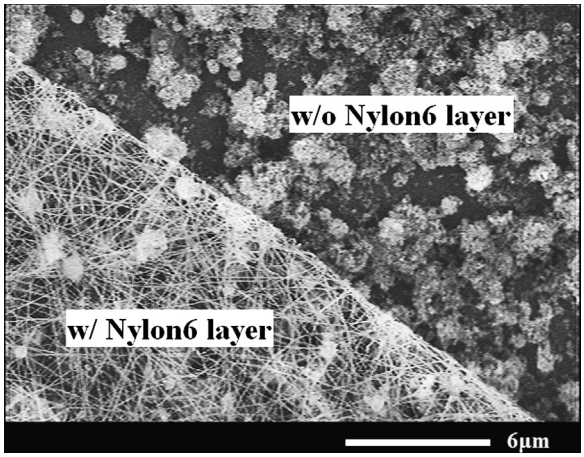

Fig. 2. SEM image of 2D structure.

Fig. 3, comparison between 3(a) and (b) shows the effect of S_1 and comparison between 3(a) and (c) shows the effect of S_2. It is apparent that the effect of S_1 on surface morphology is much more prominent than that of S_2. The size of the agglomerated particles is clearly larger in 3(b) when $S_1 = 4$ cm, as opposed to when $S_1 = 2$ cm in 3(a). The larger nozzle-to-substrate distance allows sufficient time for electrosprayed droplets to evaporate. With sufficient evaporation time under large S_1, the droplets completely evaporate prior to their deposition onto the substrate, which results in the deposition of dried and severely agglomerated nanoparticles, as in 3(b). Agglomeration is undesirable for photocatalytic activity because of reduced interfacial area of nanoparticles.

In conjunction with Fig. 3, the size distributions of the nanofibers (left column) and the nanoparticles (right column) are shown in Fig. 4. Though fiber size is little influenced by S_1 as shown in Fig. 4 (less than 5%), fiber number density has decreased when S_2 changes from 6 cm to 7 cm; compare the nanofiber size distributions from Fig. 3(a) and (c). The larger the S_2, the less the fiber number. This reduction in the fiber number is reasoned as follows: at the larger nozzle-to-substrate distance (S_2), the deposition coverage area is also enlarged, which in turn reduces the number density of nanofibers because the flowrate of the nylon-6 solution is fixed. This slight decrease in the fiber number density at larger S_2 may not be desirable because the membrane structural stability is reduced with less number of fibers that are supposed to suspend the nanoparticles. From Fig. 3(a) and (c) (right column), the size distribution of agglomerated nanoparticles is little affected by S_2. In summary, S_1 controls the evaporation process of the electrosprayed droplets, which subsequently influences the size and the photocatalytic interfacial area of titania nanoparticles. S_2 affects the structural stability because it controls the fiber number density, whose role is important to secure firm suspension of nanoparticles.

Fig. 5 shows the X-ray diffraction (XRD) patterns of the electrospun nylon-6 nanofibers, the raw TiO_2 particles, and the TiO_2-decorated nanofiber mat. The XRD pattern of the raw titania powder corresponds to 80% anatase and 20% rutile by weight, noted with A(101) and R(110), respectively. The peaks

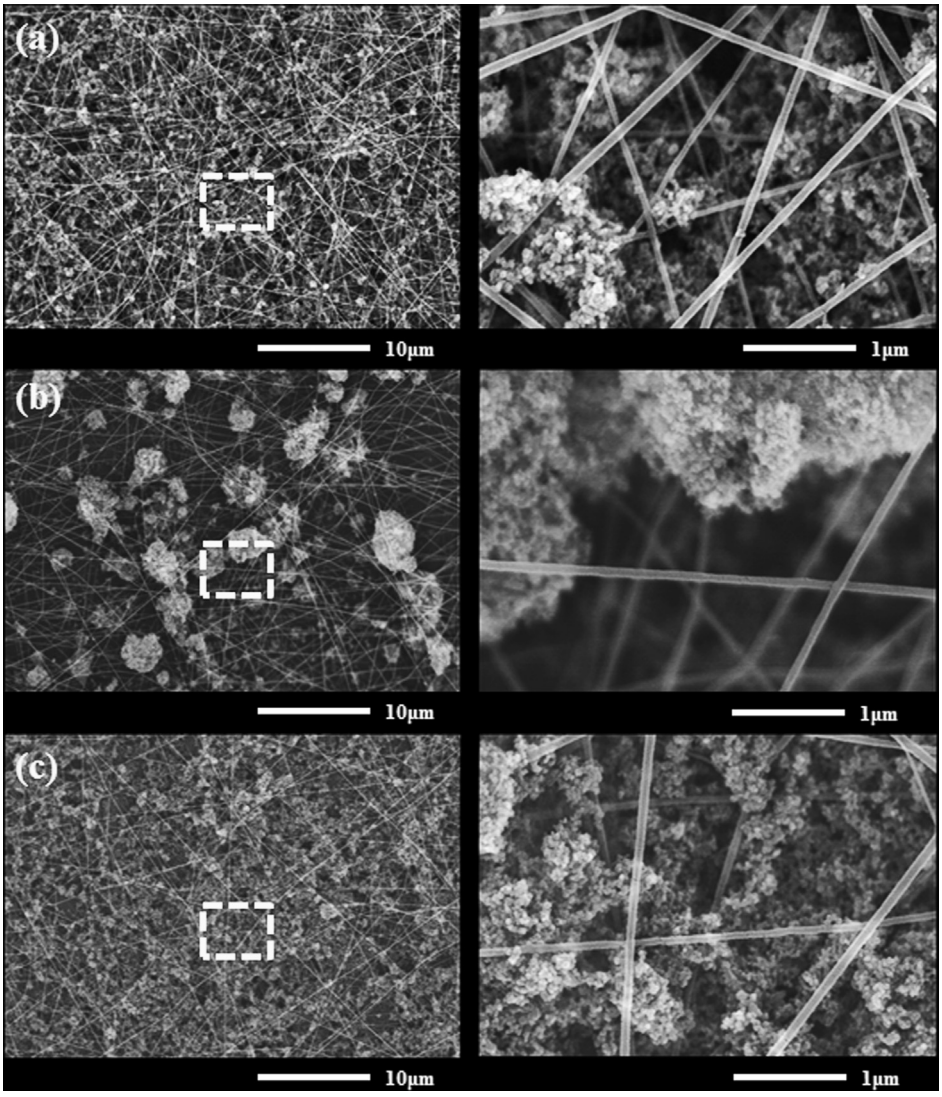

Fig. 3. SEM image of 3D structure (300 RPM, t_{dep}=5 min, nylon 15 wt%; Q=0.1 ml/h, TiO_2 3.0 wt%; Q=1 ml/h) (a) S_1=2 cm, S_2=6 cm ;(b) S_1=4 cm, S_2=6 cm and (c) S_1=2 cm, S_2=7 cm.

at 2θ=25.24° and 2θ=27.46° represent anatase and rutile, respectively [40]. In general, the anatase phase is favorable to enhance photodegradation activity. Nylon-6 is in an amorphous phase, identified with the peaks at 21.3° and 38° [41,42]. The titania-decorated nanofiber mat which consists of both TiO_2 particles and nylon-6 retains most of the peaks shown in the raw particles, but also contains the amorphous peak identified in nylon-6. The XRD result indicates that the original crystal structure of titania and nylon fiber is preserved after the coating process.

3.3. Methylene blue photodegradation test

Fig. 6 quantitatively and qualitatively compares the photocatalytic performances of the various membranes fabricated by the batch and the continuous process in terms of absorbance data over a wavelength range 400 − 800 nm under UV light illumination of t_{UV}=90 min. The greater the intensity of the transmitted light, the lower the absorbance. A lower absorbance is indicative of an increased photodegradation of the MB solution. The highest absorbance peak is observed at $\lambda \approx 664$ nm [43] which decreases as the photocatalytic reaction proceeds for t_{UV}. The peak is decreased by photo-oxidative N-demethylation of MB [36,44].

At t_{UV}=0 min, the absorbance is the highest because there is no photo-degradation activity. At t_{UV}=90 min, all of the membranes are photoactive, thus absorbance is reduced. The membrane fabricated by the batch process shows the highest absorbance because of its photocatalytic inefficiency due to the bilayer of nanoparticles and nanofibers. The bilayer is essentially a 2D structure, which significantly reduces the photoactive interfacial area of the deposited titania nanoparticles. The photodegradation performance of the 3D structure (which takes full advantage of the photoactive area of nanoparticles) is shown in the membranes fabricated by the continuous process. It is clear that photodegradation of the MB solution for the membranes fabricated by the continuous process is superior to the membranes fabricated by the batch process. For optimal case Fig. 6(c), the absorbance nears zero and the MB solution

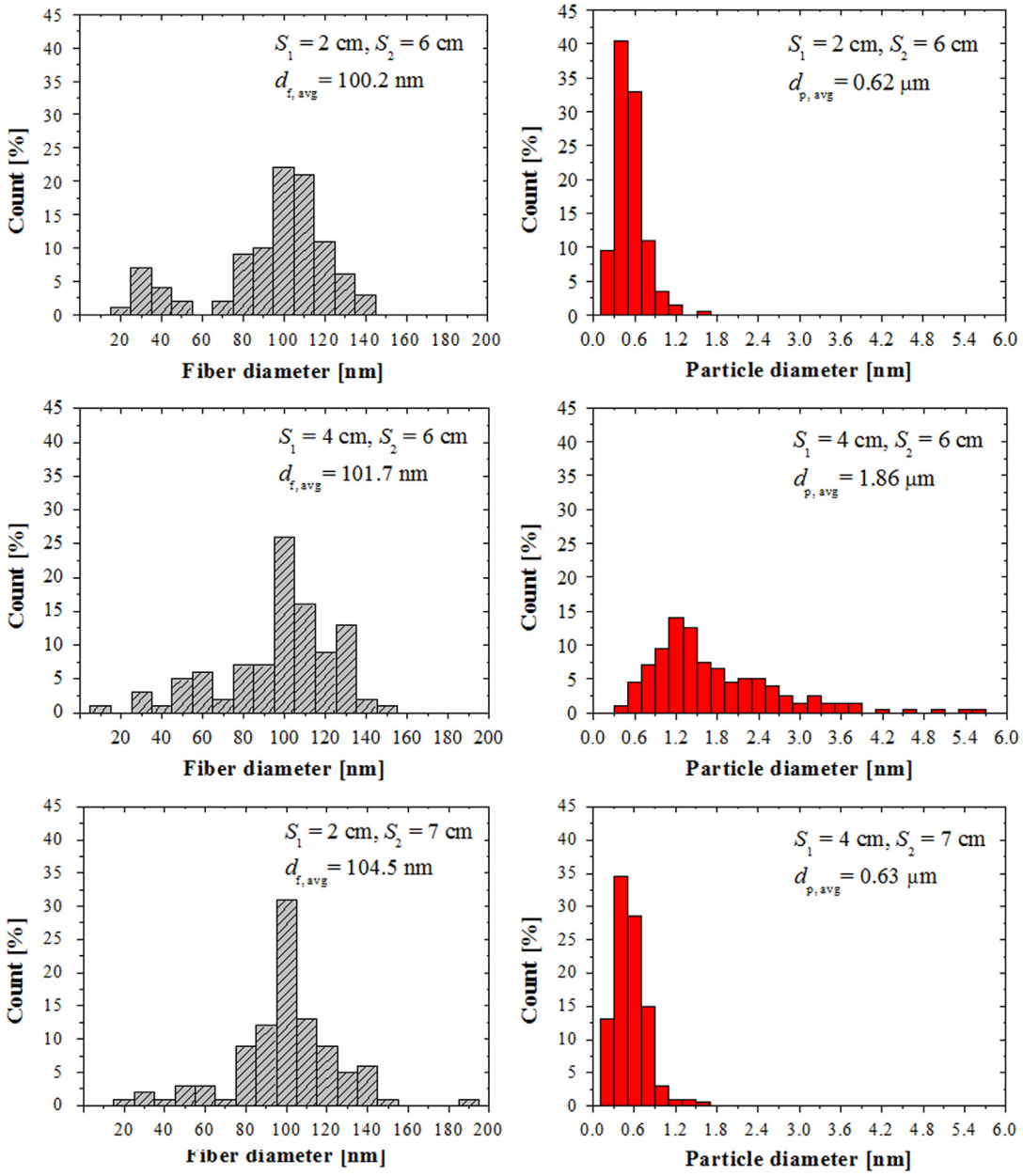

Fig. 4. The size distributions of the nanofiber (left column) and the nanoparticle (right column) for various S_1 and S_2 values.

is nearly transparent due to the strong photocatalytic activity of the 3D structure membrane.

The left inset in Fig. 6 is a snapshot of the photodegradated MB solution corresponding to lines 6(a)–(c) in Fig. 6. The far-left snapshot is the MB solution before photodegradation. The snapshots Fig. 6(b) and (c) correspond to the photodegradated MB solution from the batch and continuous processes, respectively. The result in 6(c) has the lowest absorbance or highest photodegradation performance because of the optimal nozzle-to-substrate distances (i.e., S_1 and S_2), which yielded the thinnest nanofibers and the least amount of particle agglomeration.

Table 1 shows the comparison for the photocatalytic performance of the membranes produced by our method and the method by Lombardi et al. [35]. As mentioned earlier, Lombardi et al. electrospun the nylon-6 solution comprising titania nanoparticles (P25) while our method is based on the separate deposition of nanoparticles and nanofibers via electrospraying and electrospinning, respectively. The amount of nanoparticles used in our experiment was 2.4 times less than that used by Lombardi et al. [35]. The UV light duration was $t_{UV} = 90$ min, which is smaller than what was used in Ref. [35], $t_{UV} = 170$ min. Furthermore, the intensity of our UV light was 83 times smaller than that of Ref. [35]. Nevertheless, the performance of our membrane (fabricated at $S_1 = 2$ cm and $S_1 = 6$ cm) has yielded 99.6% MB decomposition under the same initial MB concentration of 5 ppm. This demonstrates the superior photocatalytic performance of the membrane fabricated by the unique installation of electrospraying and electrospinning which takes a full advantage of the fully 3D structure of titania nanoparticles and nanofibers.

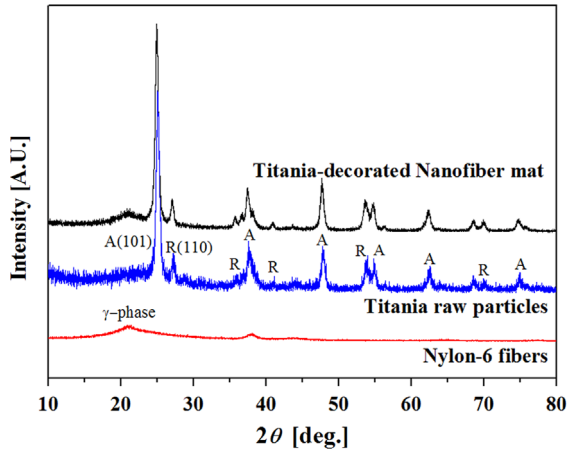

Fig. 5. XRD pattern of nylon-6, TiO_2 particles, and the antibacterial titania-decorated nanofiber mat.

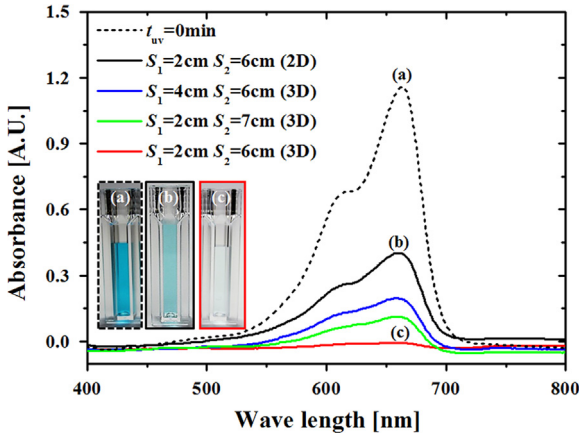

Fig. 6. Absorbance transitions from (a) methylene-blue initial concentration, (b) 2D structure, and (c) 3D structure. Note that UV light duration was t_{UV}=90 min.

The change in the MB concentration with the photocatalytic reaction time was evaluated by C/C_0 plot shown in Fig. 7, where C is the MB concentration varying as a function of the UV light duration and C_0 is the initial MB concentration. To distinguish the effect of pure adsorption and the actual photocatalytic activity, we observed the MB concentration variation without the use of any membrane while increasing the UV light duration, as shown in Fig. 7(a). Indeed, the adsorption effect is present because the MB concentration decreased with increasing t_{UV}. However, it is also clear that the adsorption effect cannot further their dilution process after $t_{UV} > 60$ min. In addition, the concentration variation is limited at nearly $C/C_0 \sim 0.6$. Further MB dilution can only be achieved by the use of our photocatalytic membranes, which clearly indicates the photocatalytic activity of our membrane, not just the adsorption phenomenon.

The 2D batch membrane corresponds to case 6(b) from Fig. 6 while the 3D continuous membrane corresponds to case 6(c) of Fig. 6. The C/C_0 results clearly show that the membrane fabricated by the continuous process produced more effective photodegradation of MB than the batch process. The Langmuir–Hinshelwood (LH) model has commonly been used to investigate the reaction kinetics of the photodegradation process. According to the LH model, kinetics of the photodegradation reaction were compared to the pseudo-first order reaction $\ln(C_0/C) = kt_{UV}$ where, k is the apparent reaction rate constant [45]. The degradation efficiency D was calculated using equation $100 \times (C_0 - C)/C_0$. Table 2 shows that the membranes fabricated by the continuous process exhibited 99.6% degradation of MB with the highest rate constant (60.5×10^{-3} min^{-1}) as compared to the membranes fabricated by the batch process.

3.4. Toxicity test of chlorophenols

Among chlorophenols (CPs), 2,4-DCP and 2,4,6-TCP are highly toxic and hardly biodegradable [46] making them difficult to remove from industrial wastewater. Thus, advanced oxidation processes (AOPs) including Fenton reaction, UV photocatalysis and ozonation have been widely used in the treatment of CPs [47,48]. As indicated in Fig. 8, acute toxicity of 2,4-DCP (5×10^{-4} M) to *D. magna* was completely reduced, starting from 2.74 TU to 0.06 TU after the photocatalytic irradiation of 3 h. In addition, this photocatalytic treatment was also effective to remove more toxic pollutant, 2,4,6-TCP (5×10^{-4} M); its toxicity was reduced from 9.85 TU to 2.78 TU. These toxicity reductions suggest that the TiO_2-decorated nanofiber membranes are effective in the treatment of industrial wastewater containing highly toxic organic compounds such as chlorophenols.

Ji et al. [48] demonstrated that reactive oxygen species including superoxide ($\bullet O_2^-$) and hydroxyl ($\bullet$OH) radicals were involved in the photocatalytic degradation of 2,4,6-TCP, which leads to dechlorination and mineralization to carbon dioxide. Gu et al. [49] also reported that 2,4-DCP was removed by both adsorption and $\bullet$OH oxidation during the photocatalytic degradation process that utilized granular activated carbon including titania particles. Shim et al. [46] showed that the oxidative degradation of 2,4-DCP and 2,4,6-TCP by the gamma-irradiation significantly reduced the acute toxicity of *D. magna*. These aforementioned studies support our finding in that the titania-decorated nanofiber mat photocatalysis is a promising candidate to remove toxic organic compounds from industrial wastewater, such as CPs.

4. Conclusions

Batch and continuous deposition processes were introduced in the membrane fabrication process and their photocatalytic water purification performances and toxicity control of chlorophenols were compared and quantified. The membrane fabricated by the batch process consisted of a bilayer of nanoparticles and nanofibers while the membrane fabricated by the continuous process suspended nanoparticles between nanofibers, thereby creating a fully 3D structure for the maximum photocatalytic performance. Furthermore, the optimal fabrication process parameters for the continuous process were identified. The nano-textured materials

Table 1
Comparison for the photocatalytic performance of the present method and that of Lombardi et al. [35].

	Present work	Lombardi et al. [35]
Deposition method	Separate installation of electrospraying P25 nanoparticles and electrospinning nylon-6	Electrospinning nylon-6 solution containing P25 nanoparticles (F10T case)
Amount of P25 nanoparticle used	0.0025 ml (=1 ml/h × 5 min × 3 wt%)	0.0030 ml (=0.12 ml/h × 15 min × 10 wt%)
Nanofiber diameter (nylon 6)	100.2∼104.5 nm	245∼278 nm
UV irradiation (duration/intensity/distance)	90 min 0.6 mW/cm^2 20 cm	170 min 50 mW/cm^2 15 cm
MB decomposition (initial conc., 5 ppm)	∼99.6% (Water solution)	80% (Ethanol solution)

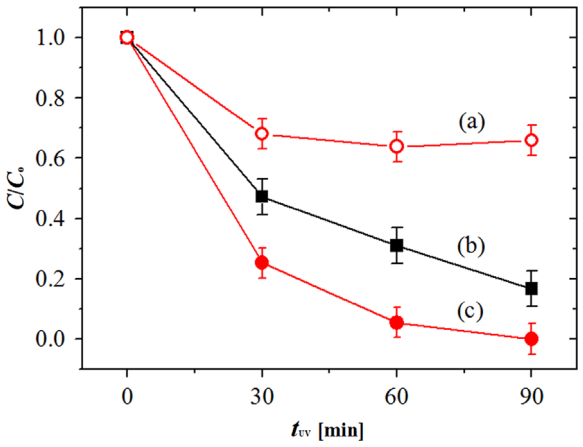

Fig. 7. (a) Blank adsorption test of the 3D membrane. Photocatalytic degradation of MB as a function of UV time by (b) 2D (batch process) and (c) 3D (continuous process) structure membranes. The 2D batch membrane corresponds to the case (b) from Fig. 6 and while the 3D continuous membrane corresponds to the case (c) of Fig. 6.

Table 2
Reaction parameters of photocatalysis for mats fabricated by batch and continuous process.

Mats	k [min^{-1} × 10^{-3}]	D [%]
Batch process	12.0	65.48
Continuous process	58.0	99.6

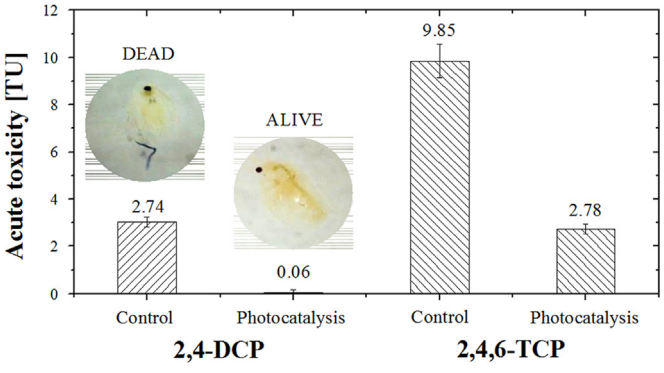

Fig. 8. Change in 48 h acute toxicity of 2,4-DCP and 2,4,6-TCP aqueous solution (5×10^{-4} M) to *D. magna* by photocatalytic treatment.

developed in this work can find practical and economical applications in water purification technology because of their simple and rapid fabrication process.

Acknowledgments

This work was supported by the National Research Foundation of Korea (2012M2B2A4029433 and 2013R1A2A2A05005589) Grant funded by the Korea Government (MEST). This research was also supported by the Converging Research Center Program through the Ministry of Education, Science and Technology (2013K000186) and the Center for Inorganic Photovoltaic Materials (No. 2012-0001169).

References

[1] M.A. Shannon, P.W. Bohn, M. Elimelech, J.G. Georgiadis, B.J. Mariñas, A.M. Mayes, Science and technology for water purification in the coming decades, Nature 452 (2008) 301–310.
[2] W.H. Glaze, J.W. Kang, D.H. Chapin, Chemistry of water treatment processes involving ozone, hydrogen peroxide and ultraviolet radiation, Ozone Science and Engineering 9 (4) (1987) 335–352.
[3] Z. Huang, P.-C. Maness, D.M. Blake, E.J. Wolfrum, S.L. Smolinski, W.A. Jacoby, Bactericidal mode of titanium dioxide photocatalysis, Journal of Photochemistry and Photobiology A: Chemistry 130 (2–3) (2000) 163–170.
[4] Q. Kang, Q.Z. Lu, S.H. Liu, L.X. Yang, L.F. Wen, S.L. Luo, Q.Y. Cai, A ternary hybrid CdS/Pt-TiO_2 nanotube structure for photoelectrocatalytic bactericidal effects on *Escherichia coli*, Biomaterials 31 (12) (2010) 3317–3326.
[5] S.D. Richardson, A.D. Thruston Jr., T.W. Collette, K.S. Patterson, B.W. Lykins Jr., J.C. Ireland, Identification of TiO_2/UV disinfection byproducts in drinking water, Environmental Science and Technology 30 (11) (1996) 3327–3334.
[6] B.R. Eggins, F.L. Palmer, J.A. Byrne, Photocatalytic treatment of humic substances in drinking water, Water Research 31 (5) (1997) 1223–1226.
[7] J.C. Yu, W. Ho, J. Lin, H. Yip, P.K. Wong, Photocatalytic activity, antibacterial effect, and photoinduced hydrophilicity of TiO_2 films coated on a stainless steel substrate, Environmental Science and Technology 37 (2003) 2296–2301.
[8] H. Lin, Z. Xu, X. Wang, J. Long, W. Su, X. Fu, Q. Lin, Photocatalytic and antibacterial properties of medical grade PVC material coated with TiO_2 film, Journal of Biomedical Materials Research Part B: Applied Biomaterials 87 (2) (2008) 425–431.
[9] V. Augugliaroa, J.B. Galvezb, J.C. Vazquezb, E.G.A. Lopeza, V. Loddoa, M.J.L. Munozc, S.M. Rodriguezb, G. Marcìa, L. Palmisanoa, M. Schiavelloa, J.S. Ruizc, Photocatalytic oxidation of cyanide in aqueous TiO_2 suspensions irradiated by sunlight in mild and strong oxidant conditions, Catalysis Today 54 (1999) 245–253.
[10] L. Armelao, D. Barreca, G. Bottaro, A. Gasparotto, C. Maccato, C. Maragno, E. Tondello, U.L. Stangar, M. Bergant, A.D. Mahne, Photocatalytic and antibacterial activity of TiO_2 and Au/TiO_2 nanosystems, Nanotechnology 18 (2007) 375709.
[11] A. Fujishima, T.N. Rao, D.A. Tryk, Titanium dioxide photocatalysis, Journal of Photochemistry and Photobiology C: Photochemistry Reviews 1 (1) (2000) 1–21.

[12] S. Singh, T. Shi, R. Duffin, C. Albrecht, D. van Berlo, D. Höhr, B. Fubini, G. Martra, I. Fenoglio, P.J.A. Borm, R.P.F. Schins, Endocytosis, oxidative stress and IL-8 expression in human lung epithelial cells upon treatment with fine and ultrafine TiO_2: role of the specific surface area and of surface methylation of the particles, Toxicology and Applied Pharmacology 222 (2) (2007) 141–151.
[13] A. Haarstrick, O. Kut, E. Heinzle, TiO_2-assisted degradation of environmentally relevant organic compounds in wastewater using a novel fluidized bed photoreactor, Environmental Science and Technology 30 (3) (1996) 817–824.
[14] I.J. Ochuma, O.O. Osibo, R.P. Fishwick, S. Pollington, A. Wagland, J. Wood, J.M. Winterbottom, Three-phase photocatalysis using suspended titania and titania supported on a reticulated foam monolith for water purification, Catalysis Today 128 (1–2) (2007) 100–107.
[15] J.M. Deitzel, J. Kleinmeyer, D. Harris, N.C. Beck Tan, The effect of processing variables on the morphology of electrospun nanofibers and textiles, Polymer 42 (1) (2001) 261–272.
[16] C.H. Hellmann, J. Belardi, R. Dersch, A. Greiner, J.H. Wendorff, S. Bahnmueller, High precision deposition electrospinning of nanofibers and nanofiber nonwovens, Polymer 50 (2009) 1197–1205.
[17] S. Megelski, J.S. Stephens, D.B. Chase, J.F. Rabolt, Micro- and nanostructured surface morphology on electrospun polymer fibers, Macromolecules 35 (2002) 8456–8466.
[18] D. Dhawale, D. Dubal, R. Salunkhe, T. Gujar, M. Rath, C. Lokhande, Effect of electron irradiation on properties of chemically deposited TiO_2 nanorods, Journal of Alloys and Compounds 499 (1) (2010) 63–67.
[19] J. Gong, X.-D. Li, B. Ding, D.-R. Lee, H.-Y. Kim, Preparation and characterization of H4SiMo12O40/poly(vinyl alcohol) fiber mats produced by an electrospinning method, Journal of Applied Polymer Science 89 (2003) 1573–1578.
[20] A. Singh, L. Steely, H.R. Allcock, Poly[bis(2,2,2-trifluoroethoxy)phosphazene] superhydrophobic nanofibers, Langmuir 21 (2005) 11604–11607.
[21] Y. Miyauchi, B. Ding, S. Shiratori, Fabrication of a silver-ragwort-leaf-like super-hydrophobic micro/nanoporous fibrous mat surface by electrospinning, Nanotechnology 17 (2006) 5151–5156.
[22] I.C. Um, D. Fang, B.S. Hsiao, A. Okamoto, B. Chu, Electro-spinning and electro-blowing of hyaluronic acid, Biomacromolecules 5 (2004) 1428–1436.
[23] H.G. Sundararaghavan, R.B. Metter, J.A. Burdick, Electrospun fibrous scaffolds with multiscale and photopatterned porosity, Macromolecular Bioscience 10 (2010) 265–270.
[24] D. Coutinho, P. Costa, N. Neves, M.E. Gomes, R.L. Reis, Tissue Engineering (2011).
[25] M.Y. Song, D.K. Kim, S.M. Jo, D.Y. Kim, Enhancement of the photocurrent generation in dye-sensitized solar cell based on electrospun TiO_2 electrode by surface treatment, Synthetic Metals 155 (2005) 635–638.
[26] M.Y. Song, D.K. Kim, K.J. Jin Ihn, S.M. Jo, D.Y. Kim, Electrospun TiO_2 electrodes for dye-sensitized solar cells, Nanotechnology 15 (2004) 1861–1865.
[27] D. Yang, X. Liu, Y. Jin, Y. Zhu, D. Zeng, X. Jiang, H. Ma, Electrospinning of poly(dimethylsiloxane)/poly(methylmethacrylate) nanofibrous membrane: fabrication and application in protein microarrays, Biomacromolecules 2009 (2009) 3335–3340.
[28] B. Carlberg, T. Wang, J. Liu, Direct photolithographic patterning of electrospun films for defined nanofibrillar microarchitectures, Langmuir 26 (4) (2010) 2235–2239.
[29] D. Wu, D. Han, A.J. Steckl, Immunoassay on free-standing electrospun membranes, Applied Materials and Interfaces 2 (1) (2010) 252–258.
[30] S.J. Cho, B. Kim, T. An, G. Lim, Replicable multilayered nanofibrous patterns on a flexible film, Langmuir 26 (18) (2010) 14395–14399.
[31] T. Lin, X. Wang, Nano related research in fibres and textiles, International Journal of Nanotechnology 6 (2009) 579–598.
[32] S. Chen, H. Hou, F. Harnisch, S.A. Patil, A.A. Carmona-Martinez, S. Agarwal, Y. Zhang, S. Sinha-Ray, A.L. Yarin, A. Greiner, U. Schroder, Electrospun and solution blown three-dimensional carbon fiber nonwovens for application as electrodes in microbial fuel cells, Energy and Environmental Science 4 (2011) 1417–1421.
[33] R. Gopal, S. Kaur, Z. Ma, C. Chan, S. Ramakrishna, T. Matsuura, Electrospun nanofibrous filtration membrane, Journal of Membrane Science 281 (2006) 581–586.
[34] X.-H. Qin, S.-Y. Wang, Filtration properties of electrospinning nanofibers, Journal of Applied Polymer Science 102 (2006) 1285–1290.
[35] M. Lombardi, P. Palmero, M. Sangermano, A.A. Varesano, Electrospun polyamide-6 membranes containing titanium dioxide as photocatalyst, Polymer International 60 (2011) 234–239.
[36] T. Zhang, T. Oyama, A. Aoshima, H. Hidaka, J. Zhao, N. Serpone, Photooxidative N-demethylation of methylene blue in aqueous TiO_2 dispersions under UV irradiation, Journal of Photochemistry and Photobiology A: Chemistry 140 (2001) 163–172.
[37] T.-D. Nguyen-Phan, V.H. Pham, T.V. Cuong, S.H. Hahn, E.J. Kim, J.S. Chung, S.H. Hur, E.W. Shin, Fabrication of TiO_2 nanostructured films by spray deposition with high photocatalytic activity of methylene blue, Materials Letters 64 (12) (2010) 1387–1390.
[38] W. Kubo, S. Kambe, S. Nakade, T. Kitamura, K. Hanabusa, Y. Wada, S. Yanagida, Photocurrent-determining processes in quasi-solid-state dye-sensitized solar cells using ionic gel electrolytes, The Journal of Physical Chemistry B 107 (18) (2003) 4374–4381.
[39] OECD, Guideline for the Testing of Chemicals: Daphnia sp. Acute Immobilisation Test, OECD 202, Organization for Economic Co-operation and Development, Paris, 2004.
[40] S.Y. Kwak, S.H. Kim, S.S. Kim, Hybrid organic/inorganic reverse osmosis (RO) membrane for bactericidal anti-fouling. 1. Preparation and characterization of TiO_2 nanoparticle self-assembled aromatic polyamide thin-film-composite (TFC) membrane, Environmental Science and Technology 35 (11) (2001) 2388–2394.
[41] D.P. Russell, P.W.R. Beaumont, Structure and properties of injection-moulded nylon-6, Journal of Materials Science 15 (1980) 197–207.
[42] A. Hosseinmardi, M. Keyanpour-Rad, A. Hesari, Impedance characteristics of electrospun nylon-6/TiO_2 nanocomposite for humidity sensor, Key Engineering Materials 471–472 (2011) 542–547.
[43] C. Yogi, K. Kojima, N. Wada, H. Tokumoto, T. Takai, T. Mizoguchi, H. Tamiaki, Photocatalytic degradation of methylene blue by TiO_2 film and Au particles-TiO_2 composite film, Thin Solid Films 516 (17) (2008) 5881–5884.
[44] Y. Sakatani, D. Grosso, L. Nicole, C. Boissiere, G.J. de AA Soler-Illia, C. Sanchez, Optimised photocatalytic activity of grid-like mesoporous TiO_2 films: effect of crystallinity, pore size distribution, and pore accessibility, Journal of Materials Chemistry 16 (1) (2006) 77–82.
[45] Y. Zhang, J. Wan, Y. Ke, A novel approach of preparing TiO_2 films at low temperature and its application in photocatalytic degradation of methyl orange, Journal of Hazardous Materials 177 (2010) 750–754.
[46] S.B. Shim, H.J. Jo, J. Jung, Toxicity identification of gamma-ray treated phenol and chlorophenols, Journal of Radioanalytical and Nuclear Chemistry Articles 280 (2009) 41–46.
[47] M. Pera-Titus, V. Garcia-Molina, M.A. Banos, J. Gimenez, S. Esplugas, Degradation of chlorophenols by means of advanced oxidation processes: a general review, Applied Catalysis B 47 (2004) 219–256.
[48] H. Ji, F. Chang, X. Hu, W. Qin, J. Shen, Photocatalytic degradation of 2,4,6-trichlorophenol over g-C_3N_4 under visible light irradiation, Chemical Engineering Journal 218 (2013) 183–190.
[49] L. Gu, Z. Chen, C. Sun, B. Wei, X. Yu, Photocatalytic degradation of 2, 4-dichlorophenol using granular activated carbon supported TiO_2, Desalination 263 (1) (2010) 107–112.